INSTITUTE OF PHYSICS PUBLISHING and INTERNATIONAL ATOMIC ENERGY AGENCY NUCLEAR FUSION

Nucl. Fusion **45** (2005) 685–693 doi:10.1088/0029-5515/45/7/018

Effects of wall boron coating on FTU, an all metallic and carbon free medium size tokamak

M.L. Apicella[1], G. Mazzitelli[1], B. Esposito[1], L. Gabellieri[1], M. Leigheb[1], V. Pericoli Ridolfini[1], L. Pieroni[1], M. Romanelli[1], R. Zagórski[2] and FTU team

[1] Associazione EURATOM-ENEA sulla Fusione, Centro Ricerche di Frascati, C.P. 65-00044 Frascati, Rome, Italy
[2] Institute of Plasma Physics and Laser Microfusion, PO Box 49, PL-00-908, Warsaw, Poland

Received 16 September 2004, accepted for publication 16 May 2005
Published 30 June 2005
Online at stacks.iop.org/NF/45/685

Abstract
Boronization of FTU tokamak strongly affects its gas recycling, impurity concentration and its temporal evolution. Two main phases are distinguished. In the first one, lasting about 60 discharges, with the machine fully boronized, the radiation losses decrease from 80% to 40% and the impurity content drops from $Z_{\rm eff} = 6$ to $Z_{\rm eff} \approx 1.5$ at $\bar{n}_{\rm e} \approx 0.35 \times 10^{20}\,{\rm m}^{-3}$ in ohmic conditions. In the second phase, lasting >500 discharges, with the B film eroded from the TZM toroidal limiter surface but not from the SS walls, the reduction of radiated power (≈60%) and impurities ($Z_{\rm eff} \approx 2.0$) though smaller, is still important with respect to pre-boronization, allowing for optimization of plasma characteristics up to the maximum RF power so far injected (2.6 MW ≈ 1.6 MW m^{-3}). The recycling properties of the B film are fully stabilized, making the plasma operations much more reliable, while the gettering properties are preserved and they maintain the oxygen below $n_{\rm O} \leqslant 0.5\%$.

PACS numbers: 52.40.Hf

(Some figures in this article are in colour only in the electronic version)

1. Introduction

Most of the present tokamaks operate at a relatively low density and use graphite or carbon composites as first wall material. Graphite is known for its good thermo-mechanical properties and low atomic number. However, the control of oxygen inventory and its release in the plasma as H_2O, CO and CO_2 molecules has been a big problem for these machines. To reduce plasma contamination, a large effort has been made to optimize cleaning and conditioning procedures, which have led, as a final step, to cover *in situ* the vacuum chamber with boron [1–5] and silicon coatings [2, 6]. These materials are, in fact, very suitable as their properties form tight bonds with oxygen and carbon. As a consequence of their use, plasma contamination and gas recycling have been strongly reduced leading to a significant improvement in plasma performances.

The boronization technique has also been applied on FTU ($R = 0.93$ m, $a = 0.33$ m, $B_{\rm T} \leqslant 8$ T, total pulse duration $t_{\rm pulse} \approx 1.5$ s), which uses a molybdenum alloy (TZM) for the internal toroidal limiter and the external poloidal limiter and stainless steel AISI 304 for the vacuum chamber walls. The first boronization on an all-metallic tokamak was carried out on Alcator C-Mod [7], which belongs to the same class of the high field, high density ($\bar{n}_{\rm e} > 1 \times 10^{20}\,{\rm m}^{-3}$) compact devices as the FTU [8] and uses molybdenum as the first wall material. This technique has permitted the production of a stable H-mode transition [9] by reducing carbon and oxygen fluxes coming from the Mo tiles. Light impurities, in fact, increase the production of molybdenum by physical sputtering, which, in turn, prevents the maintenance of H-mode.

On our machine it is possible to assess better the effects of boron coating on a true Mo first wall, because carbon concentration inside the plasma is negligible and that of oxygen is small for well-cleaned walls.

The peculiar feature of FTU of operating in a wide density range $\bar{n}_{\rm e} = 0.3$–$3.2 \times 10^{20}\,{\rm m}^{-3}$ allows the study of very different plasma regimes both in the ohmic and in heated plasmas with lower hybrid (LH) and/or electron cyclotron (EC) waves (up to 2.6 MW of total RF power injected) without major problems arising from the use of high Z materials. This is due to the high power density and the high-density regimes that are possible on the FTU. The high power density enables the plasma to support a relatively large amount of metallic impurities before the local radiation losses exceed

the input power density. The high density, instead, reduces the temperature at the plasma edge, thus reducing the physical sputtering yields of metals.

Following an opening to the air in the vacuum vessel, baking of 3–4 days up to 393–413 K is sufficient to achieve a good wall conditioning. Water vapour is the main gas desorbed from the metallic surfaces, whereas CO and CO_2 are negligible in comparison. After baking, the machine is cooled to the operating temperature of $T_w \approx 77$ K. Such a conventional technique leads to an oxygen concentration of 1.0–1.5% after about 100 plasma discharges. In this case values less than 1% are very difficult to obtain. Heavy impurity contamination at high density ($\bar{n}_e \geqslant 1.0 \times 10^{20}\,m^{-3}$) and current (1.0 MA) is negligible because the metal influx by O-sputtering is sufficiently low. Effective ion charge values (Z_{eff}) less than 2 and total radiated power ≈70% of the input power are usually achieved. However, at lower plasma density, i.e. at $\bar{n}_e = 0.3 \times 10^{20}\,m^{-3}$, we never obtain Z_{eff} less than 6 even with well-cleaned walls. This behaviour is typical of a metallic first wall machine, as described in [10].

Before the installation of the toroidal limiter, wall siliconization was studied to assess the specific role of oxygen in high-density regimes with fully metallic first walls. Experiments were also carried out where the material of the full poloidal limiter was changed from low Z (silicon coated Mo) to medium Z (Ni) and high Z (Mo and W). The highest density limit was obtained after siliconization, when silicon was eroded by the Mo limiter, but it was still present on the vessel walls: ($\bar{n}_e = 3.2 \times 10^{20}\,m^{-3}$) at $I_p = 0.7$ MA, $B_T = 6$ T, which is a factor 1.3 higher than that predicted by the Greenwald limit. Very low oxygen concentration in the plasma was found in that case ($n_O \leqslant 0.5\%$). In the case of a silicon coated limiter, in the phase immediately after siliconization, a lower density limit was obtained and no reduction of Z_{eff} value at low density was achieved owing to the large silicon influx into the plasma core. All these results are well documented in [10, 11] in terms of the radiation losses characteristics, the nature of the limiter material and the mechanism of impurity production. These experiments have pointed out the importance of limiting the light impurity concentration (mainly oxygen) in order to achieve operations at the maximum performance in FTU.

As a first step towards optimizing plasma operations after the installation of the toroidal limiter, a 'titanization' technique was tested on FTU [12]. A thin Ti layer was deposited onto the vessel walls by evaporating a small amount of titanium between discharges (≈5 monolayers). This conditioning technique promptly allows the maintenance of a very low oxygen concentration at high densities (with $Z_{eff} \approx 1.0$ for $\bar{n}_e \geqslant 1.0 \times 10^{20}\,m^{-3}$) and at low density ($Z_{eff} \approx 4.4$ at $\bar{n}_e = 0.3 \times 10^{20}\,m^{-3}$). It is a very efficient tool for minimizing oxygen contamination in case of small vacuum leaks, but Z_{eff} cannot be reduced below 4 at low density owing to the high Ti atomic number ($Z_{Ti} = 22$). The second step in optimizing FTU operations has been to exploit the 'boronization' technique [13].

In this paper, a brief description of the experimental apparatus and of the boronization procedure is given in section 2 followed by the analysis of the effects of boronization on the plasma characteristics in section 3. This includes all the physical aspects related to the main plasma as well as an investigation of the Scrape-Off-Layer (SOL) using a two-dimensional model of the energy and particle transport. Section 4 describes how boronization can affect the recycling properties and the density control. Finally, conclusions are drawn in section 5.

2. Experimental apparatus and boronization procedure

Since October 2001, a large number of boronizations have been carried out using a dc-glow discharge in a throughflow of 90% of helium and 10% of diborane B_2H_6 (since September 2002, B_2D_6 was used to avoid plasma dilution by hydrogen). During boron deposition, the wall temperature is maintained at 298–373 K to assure a good adherence of the film to the substrate. Major modifications with respect to the standard dc-glow discharge have been made in the gas inlet system and in the evacuation lines to assure the safe handling of a hazardous gas as diborane [14]. The geometrical configuration of the gas inlet system and of the gas evacuation lines has been optimized to obtain a boron deposition, which is as uniform as possible. The gas mixture is introduced through four vertical ports located 90° toroidally apart from each other, at a pressure of about 7×10^{-3} mbar with 1.7 mbar l s^{-1} of average gas flow rate. The gas is pumped away using two evacuation lines of the main vacuum system placed at two opposite sides of the torus. Each line is connected to a standard 2000 l s^{-1} turbomolecular pump, followed by a thermal decomposer. The annexed 60 m^3 h^{-1} rotary pump is modified to assure a very good vacuum tightness and to dilute the exhaust gas with nitrogen before it comes in contact with air. Two electrodes, 180° toroidally apart, are inserted from two vertical ports up to the centre of the vacuum chamber. The glow discharge conditions for each electrode are a voltage drop of +360 V towards the wall at ground potential and a driven current of 0.75 A, corresponding to 11 μA cm^{-2} of total current density onto the vessel walls. Unlike other tokamaks, where the film thickness can be easily evaluated by visual inspection or by inserting samples in different positions of the vacuum chamber [1, 15], FTU is a compact machine with few narrow accesses, which do not permit an accurate investigation of the film uniformity. To evaluate the best operating parameters for boron deposition, preliminary laboratory tests have been performed using one spare sector of the FTU machine [16]. In this case, the film thickness was estimated to be about 100 nm for 3 h of boronization as a result of the differences in the post- and pre-deposition weight of different samples of SS 304, with the same mechanical surface treatment as the FTU walls.

In figure 1 the spectrum of quadrupole mass analyser (QMA) during the boronization process is shown. The QMA does not detect diborane (B_2D_6) at mass 34 because this molecule is broken in many radicals on the QMA filament. The most important fragments are found at masses 32 ($B_2^{11}D_5$) and 31 ($B^{10}B^{11}D_5$), which are used as markers of the diborane partial pressure.

During the FTU operations the only signals that are detectable on the QMA are D_2, N_2 and O_2 (see figure 2(*a*)). The presence of N_2 at cryogenic temperature is due to a low leakage from the cryostat, which has no effect on FTU plasma discharges. In this phase the mass analyser cannot be used for

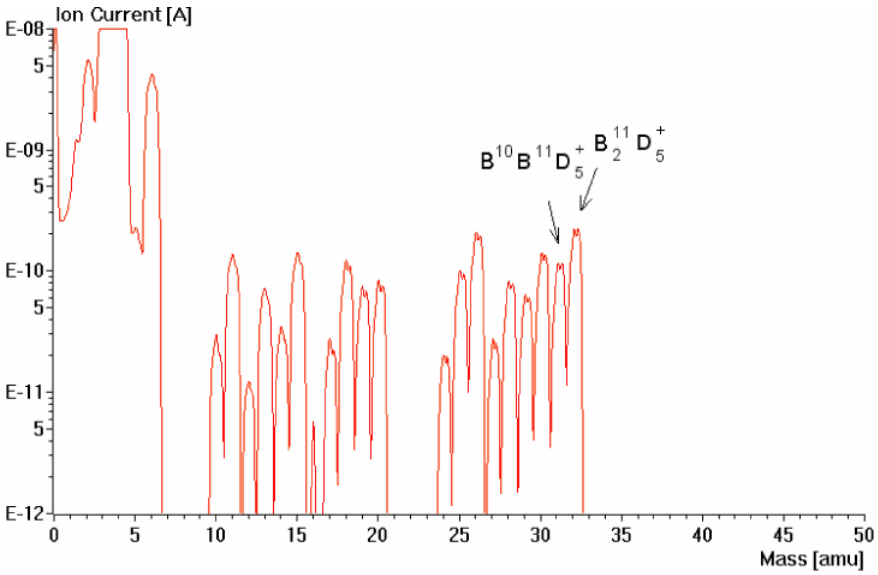

Figure 1. Mass spectrum of QMA during the boronization process.

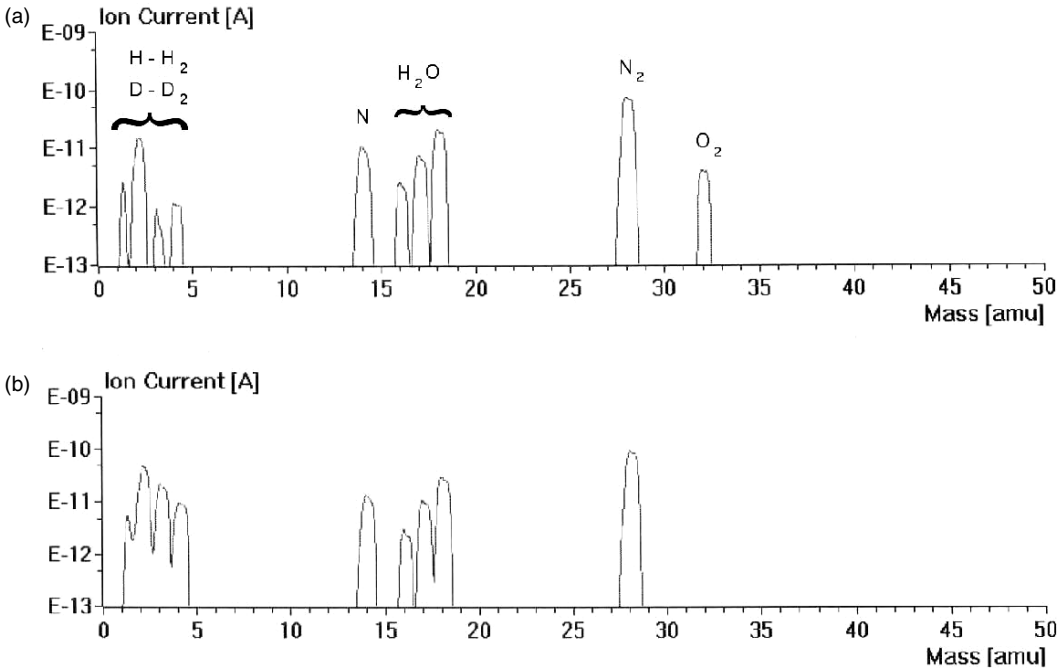

Figure 2. Mass spectra at cryogenic temperature (*a*) before and (*b*) during the experimental session. Oxygen disappears after a few plasma discharges.

water vapour because it is trapped by the cold walls (some sort of extended cryogenic pumping), and the H_2O signal shown in figure 2(*a*) is only due to the quadrupole background. For this reason neither the outgassing rate nor the equilibrium pressure give useful information on monitoring the state of cleanliness of the chamber walls during the experimental campaign.

Typically, after boronization, oxygen disappears from the mass spectrum (see figure 2(*b*)) after 1–2 plasma discharges. This phenomenology is probably because of the bonding of the recycled oxygen in a more stable oxide, boron oxide, in the boron-coated walls. Only after two or three days from the end of the experimental session does the oxygen level revert to its previous value owing to the slow outgassing rate from the surfaces not exposed to the plasma.

It is found that, after boronization, the boron layer does not pump molecular oxygen if it is not activated before by a few plasma discharges, as observed in the past on ASDEX [15].

3. Plasma characteristics

After a fresh boronization, the restart of operations is immediate (1–2 discharges) and the recovery from plasma disruptions is prompt as in the case of a pure metallic machine without any contamination of light impurities (O and C). The production of plasma discharges is easier than for standard

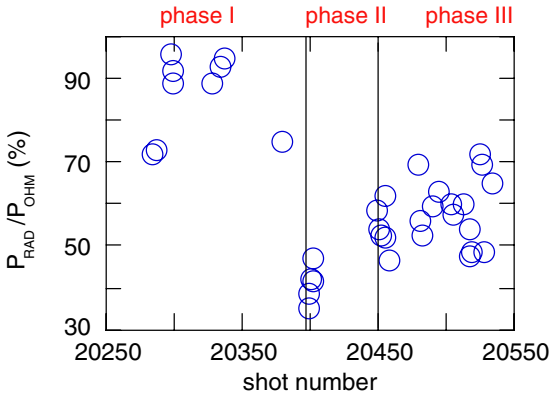

Figure 3. Fraction of the radiated power P_{RAD} to the ohmic power P_{OHM} (in per cent) as a function of the shot number for ohmic discharges with $I_p = 0.5$ MA and $\bar{n}_e = 0.3$–0.8×10^{20} m^{-3}.

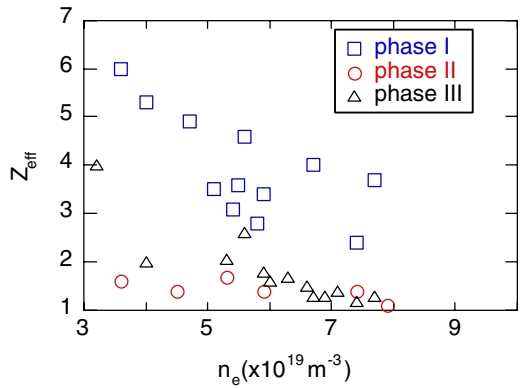

Figure 4. Experimental Z_{eff} against the average electron density before (phase I), immediately after (phase II) and at long time distance from boronization (phase III) for the same discharges of figure 3.

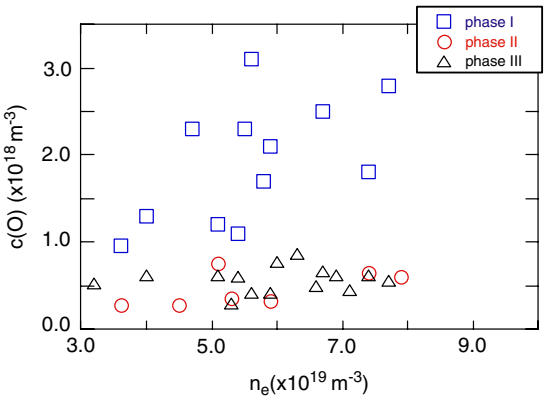

Figure 5. Oxygen concentration in the plasma as a function of the average electron density for the same discharges of figure 3. Very low values are also obtained after 500 discharges after boronization.

conditions owing to the more favourable emission properties of low Z impurities, which are totally ionized in the plasma centre and thus prevent the onset of hollow temperature profiles.

3.1. Radiative losses and impurity behaviour

There are two main effects of boronization on the bulk plasma characteristics. In an ohmic plasma ($\bar{n}_e = 1.0 \times 10^{20}$ m^{-3}) the total radiated power typically falls from 70–90% to 35–40%, and for $I_p = 0.5$ MA and $\bar{n}_e = 0.35 \times 10^{20}$ m^{-3}, Z_{eff} decreases from 6.0 to 1.6. This is due to the strong reduction of heavy metal concentrations, which in the case of molybdenum drops from 6 to 1.2×10^{16} m^{-3} at $\bar{n}_e = 0.35 \times 10^{20}$ m^{-3}, and to the better action of boron on the light impurities. This latter reduces the oxygen concentration in the plasma from 2.5% to 0.5% and the carbon flux from the walls from 1.0×10^{18} to 1.1×10^{17} particles s^{-1} m^{-2}. The radiation losses from the outer plasma ($r/a = 0.8$–1.0) decrease by more than a factor 2 at low density consistently with a strong reduction of the light impurities, whose contribution dominates at the plasma periphery. The experimental values of the radiative losses, Z_{eff} and impurity concentration are well reproduced by a one-dimensional impurity transport code by assuming an anomalous diffusion coefficient and an inward velocity equal to the usual FTU ohmic values [17]. As a consequence of the Z_{eff} reduction, the resistivity and hence the loop voltage are lower for the same plasma current. The smaller input power reduces, in turn, the electron temperatures up to 1.3 times.

All these effects last approximately 60 discharges corresponding to the duration of the boron coating on the limiter, as inferred by the reappearing of the molybdenum lines on the UV spectra. To better understand the evolution of plasma behaviour, we have compared ohmic discharges with $I_p = 0.5$ MA and $\bar{n}_e = 0.3$–0.8×10^{20} m^{-3} during three temporal phases characterized by different wall conditions: phase I, corresponding to the standard operations (TZM limiters and SS wall) at the beginning of the experimental campaign after baking; phase II, immediately after boronization (boronized limiter and walls) and phase III at long time distance from boronization (TZM limiters and boronized walls). The transition between the different phases is easily recognized by the evolution of the radiated/ohmic power ratio (figure 3). This ratio decreases from about 70–90% (phase I) to 40% (phase II) and then slowly increases again during phase III but not to the pre-boronization values, indicating a plasma contamination lower than before boronization. Clear evidence comes from the total impurity content expressed as Z_{eff} and the concentration of oxygen n_O shown in figures 4 and 5. Both these parameters drop immediately after boronization, owing to the strong reduction of heavy metals and oxygen concentration. In the third phase when boron has been eroded from the limiter but is still present on the chamber walls, i.e. after about 60 discharges, the oxygen concentration does not increase at all and the metal concentration is lower than before boronization, because the physical sputtering by oxygen ions and atoms is strongly reduced. As a consequence, the Z_{eff} values are lower than before boronization. During this phase, which lasts for 500 discharges at least, the metal influx can be further reduced by cooling the plasma edge with a deuterium puff immediately before the start-up of a plasma discharge.

In these conditions, with molybdenum as the main impurity and very low oxygen contamination, the reduction of Z_{eff} has allowed the FTU to reach one of its best performances, in terms of current drive (CD) efficiency η_{CD} (#21640). Full CD with $\eta_{CD} = 0.18 \times 10^{20}$ A m^{-2} W^{-1} (which becomes $\approx$0.26 if reduced to $Z_{eff} = 1$ case) [18] has been obtained on a plasma target with: $I_p = 0.36$ MA, $B_T = 5.3$ T,

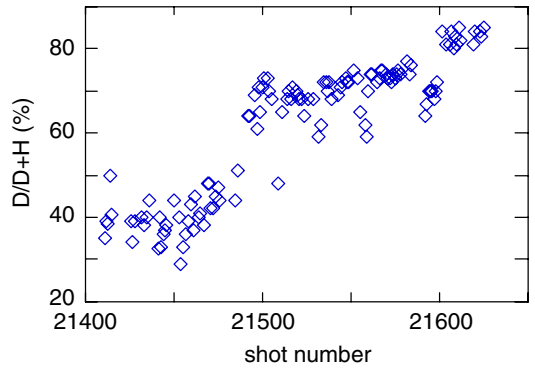

Figure 6. Ratio of deuterium to deuterium + hydrogen fluxes as a function of shot number starting from the first discharge after boronization (# 21411).

$\bar{n}_e = 0.4 \times 10^{20}\,m^{-3}$ and $P_{LH} = 1.5\,MW$, with only a small increase of Z_{eff} from 1.5 to 2.2. With the same plasma target, the maximum additional power so far injected, i.e. $P_{LH+EC} = 2.6\,MW$, has raised Z_{eff} to 3.0 (#21636), whereas a lower power ($\sim$1 MW) has given $Z_{eff} = 6.0$ before boronization.

3.2. Plasma dilution and energy confinement time

A consequence of boronizations carried out with B_2H_6 as the feeding gas is a large dilution of the D-plasma with the hydrogen particles released from the B film. The ratio of deuterium to deuterium + hydrogen fluxes $q_D/(q_D + q_H)$, as measured by the neutral particle analyser, can be as low as 40% after a fresh boronization, despite the pure D_2 puffing, which then increases slowly to 85% after about 200 discharges, as shown in figure 6, starting from the first shot after boronization (#21411). The D dilution, in turn, reduces the plasma performances in terms of the neutron yield. The target plasma suitable for pellet injection ($\bar{n}_e = 1.7 \times 10^{20}\,m^{-3}$) shows a decrease of the neutron rate up to a factor 5 in spite of the much lower radiated power than before boronization ($P_{RAD}/P_{OHM} \approx$ 35% against 65%, together with $Z_{eff} \approx 1$ against $Z_{eff} \approx 1.4$).

To overcome the problem of D dilution, boronizations with deuterate diborane B_2D_6 have been successfully tested. Nevertheless, experimental results show that the suppression of plasma dilution does not lead to the total recovery of the neutron rate to the pre-boronization values, as evidenced in figure 7 for two ohmic discharges with $I_p = 0.5\,MA$, $B_T = 6.0\,T$ and $\bar{n}_e = 0.5 \times 10^{20}\,m^{-3}$ obtained before (#20286) and after boronization with B_2D_6 (#22862). The difference is a consequence of the Z_{eff} reduction after boronization, which produces an input power and consequently an electron temperature lower than before boronization. In the same figure, for comparison, the neutron rate obtained after boronization with B_2H_6 (#20401) is plotted to show the effect of the plasma dilution.

The effects of boronization on the energy transport properties have been investigated by means of the one-dimensional transport code EVITA[1], which is currently used on FTU to analyse discharges in different plasma conditions and heating scenarios [19].

The code EVITA applied to the B_2D_6 case well reproduces the experimental neutron rate assuming a pure deuterium

[1] Zanza V. http://efrw01.frascati.enea.it/Software/Unix/FTUcodici/evita.

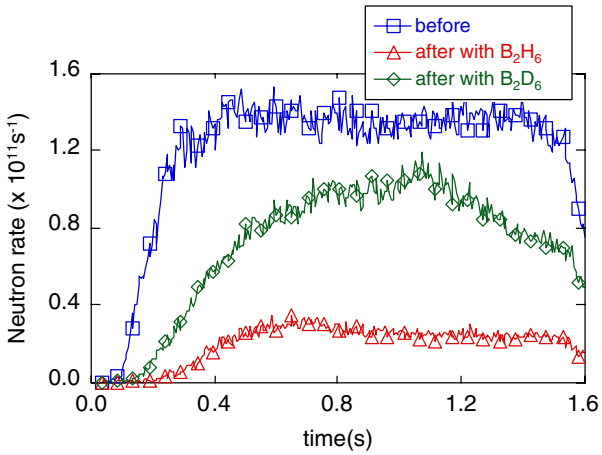

Figure 7. Comparison of neutron generation rate for three plasma discharges: the first one obtained before boronization (#20286), the second one after boronization with B_2H_6 (#20401) and the third one after boronization with B_2D_6 (#22862). In all the cases $\bar{n}_e = 0.5 \times 10^{20}\,m^{-3}$, $I_p = 0.5\,MA$, $B_T = 6\,T$.

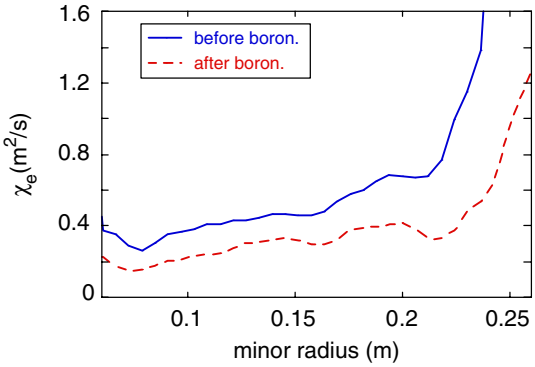

Figure 8. Radial profile of electron heat conductivity for two plasma discharges before (#20286) and after (#22864) boronization with B_2D_6.

plasma and the same ion transport coefficient used for similar discharges before boronization. The main effect of boronization on the transport properties is the improvement of the energy confinement time τ_E by a factor 1.35. This is due to the ohmic power reduction, whereas the total thermal energy remains nearly constant. This means that a lower input power is sufficient to obtain the same plasma energy. The electron transport coefficient χ_e is consistently lower, as shown in figure 8 for two ohmic plasma discharges at $\bar{n}_e = 0.5 \times 10^{20}\,m^{-3}$ and $I_p = 0.5\,MA$ before (#20286) and after (#22864) boronization with B_2D_6.

If we compare the confinement time with ITER97L scaling law [20], τ_E after boronization results 1.14 times higher, according to the EVITA code analysis. This value, in addition, is definitely higher than the average value for the standard FTU ohmic discharges, which is $\tau_E/\tau_{ITER97L} = 0.92$ [19].

3.3. Density limit

High-density plasmas are obtained with fresh and old boronization with gas puffing only. The density limit at $I_p = 1.1\,MA$, $B_T = 7.2\,T$ reaches a value of $\bar{n}_e = 3.2 \times 10^{20}\,m^{-3}$,

twice that of before boronization and corresponding to 0.8 times the Greenwald limit. After boronization only oxygen and hydrogen radiation lines are present in the UV spectrum with $Z_{\rm eff}$ close to 1.0.

The role of oxygen at high density has been assessed by comparison between the experimental results and those predicted by a simple model based on a zero-dimensional description of the bulk plasma and one-dimensional modelling of the plasma transport in the SOL [21]. Only two different types of impurities are supposed to be present in the plasma: the first is the sputtered impurity produced at the limiter (boron or molybdenum), the second is introduced as a percentage of the electron density (oxygen) and is independent of the plasma parameters. The density limit occurs in the code when the total radiation $P_{\rm RAD}/P_{\rm OHM}$ approaches 100%, and no steady state solution exists in the model equations. This condition was found to appear at progressively higher electron density as the oxygen concentration is lowered and is independent of limiter material. In fact, close to the density limit, the temperature on the limiter surface is so low that the sputtering processes are strongly reduced and the limit is defined by the radiation of the second impurity (oxygen) and of hydrogen.

The role of the different limiter materials can be qualitatively explained by the physics of MARFE. This thermal instability always precedes the density limit on FTU [22] and is strictly related to the cooling rate characteristics of low-Z impurities at the edge plasma [23]. This quantity shows a strong inverse dependence on the electron temperature which can lead to a MARFE if the heat flux transported along the magnetic field lines cannot compensate for the local radiation losses. According to the impurity characteristics, MARFE cannot be attributed to boron and molybdenum but to the small presence of oxygen in the discharge. Molybdenum, in fact, shows a peak of the cooling rate shifted inside the plasma (at about 1 keV), so that it cannot develop an unstable region at the edge. The cooling rate of boron, instead, is mostly confined at very low electron temperatures in the SOL region, peaks at 3 eV and does not affect the thermal equilibrium of plasma. These results are not in contrast with those obtained in the past with silicon as dominant impurity [11]. In that case, in fact, the behaviour of the plasma was very similar to that obtained with oxygen as a dominant impurity. For increasing density, silicon was found to irradiate inside a large region of the external plasma ($0.8 \leqslant r/a \leqslant 1$), thus leading to an early onset of MARFE and then to the plasma disruption, with a phenomenology very similar to that of oxygen. With boron and molybdenum as first wall materials, the effect of boronization on oxygen reduction implies the highest density limit, as was experimentally observed.

3.4. SOL characteristics

An investigation of the SOL characteristics has been possible only at low electron density ($\bar{n}_{\rm e} = 0.45 \times 10^{20}\,{\rm m}^{-3}$) where reproducible plasma conditions are achieved. According to Langmuir probe measurements, $n_{\rm e}$ and $T_{\rm e}$ profiles in the SOL are uniform in post-boronization discharges at the four poloidal positions. No variation is detected, whether the limiter is still B-coated (phase II) or the B film has already been eroded (phase III).

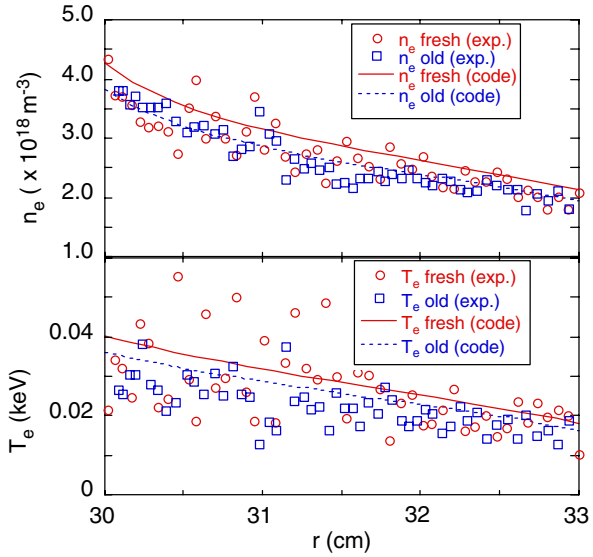

Figure 9. Experimental (symbols) and code (lines) radial profiles of electron density (first frame) and electron temperature (second frame) in the SOL plotted against the minor radius after a fresh boronization (#22871) and after an old boronization (#23186). For both discharges $\bar{n}_{\rm e} = 0.45 \times 10^{20}\,{\rm m}^{-3}$ and $\theta = 240^{\circ}$ measured from the outer equatorial plane in the counter-clockwise direction.

In figure 9 the SOL electron density and temperature profiles, measured by the Langmuir probe closest to the limiter, 30° poloidally away from the limiter ($\theta = 240^{\circ}$), are compared (with open symbols) for two ohmic discharges: the 13th and the 328th after boronization. In both cases the $n_{\rm e}$ and $T_{\rm e}$ values at the last closed magnetic surface (LCMS) are nearly the same as the radial decay lengths across the SOL. The density and temperature e-folding lengths calculated with reference to the magnetic flux surfaces of the external equatorial plane give the following results: $\lambda_{\rm n} = 1.9\,{\rm cm}$ and $\lambda_{\rm T} = 1.9\,{\rm cm}$ for fresh boronization and $\lambda_{\rm n} = 1.6\,{\rm cm}$ and $\lambda_{\rm T} = 2.1\,{\rm cm}$ for old boronization. In the same figure the SOL profiles for $n_{\rm e}$ and $T_{\rm e}$ calculated with the two-dimensional multifluid code EPIT [24, 25], are also shown in good agreement with the experiment.

The recycled fluxes, as given by D_α emission on different horizontal and vertical chords shown in figure 10, are also very similar in the two discharges. Only the input energy flux into the SOL ($P_{\rm SOL}$) is different, being higher by a factor of 1.5 for the shot with fresh boronization owing to the lower radiating losses. This confirms that changes of $P_{\rm SOL}$ in FTU are often too small to affect the electron temperature beyond the experimental accuracy, as previously found in [26] where the SOL characteristics with fully metallic walls are discussed. The constancy of $n_{\rm e}$ in the SOL is instead a natural consequence of the unchanged core plasma average density and profile and the similar recycling characteristics.

The input quantities for the EPIT code, related to the energy and particle transport within the SOL, have been adjusted in order to reproduce the experimental profiles. These values are well within the usual range of variability for FTU; see [27] where more details on the code and the calculations are given. The code shows that parallel heat conductivity, $\chi_{\rm e}$, of the electrons is mainly responsible for the limited variation of $T_{\rm e}$ from phase II to phase III, about 10%, i.e. $\Delta T_{\rm e} \approx 4\,{\rm eV}$

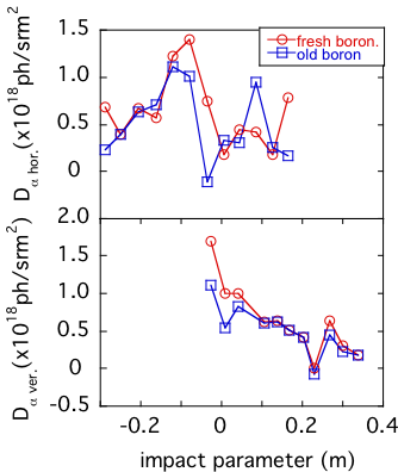

Figure 10. D_α emission along horizontal and vertical chords plotted as a function of the impact parameter for wall conditions immediately after boronization (#22871) and at long time distance from boronization (#23186).

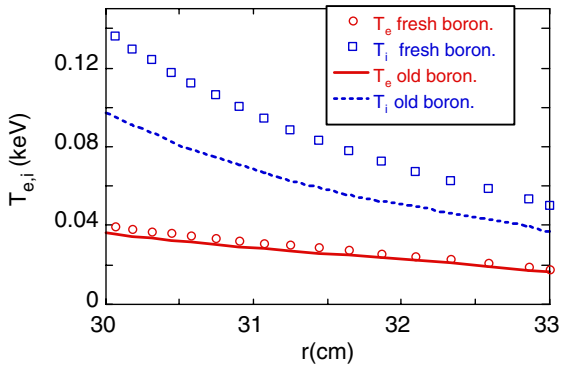

Figure 11. Predicted T_i and T_e radial profiles in the SOL for $\vartheta = 240^\circ$ starting from the LCMS down to the wall position after a fresh boronization (#22871) and after an old boronization (#23186). For both discharges $\bar{n}_e = 0.45 \times 10^{20}\,m^{-3}$, $I_p = 0.5$ MA and $B_T = 6$ T.

(see figure 9). Indeed, the rapid increase of χ_e with T_e ($\chi_e \propto T_e^{5/2}$) can accommodate significant variation of the input power into the SOL with only limited changes of T_e. In addition, the line radiation contributes non-negligibly to the stabilizing $T_{e,SOL}$ when the density limit is approached, for cases of B or Mo dominant impurity. Therefore, for the typical FTU parameters EPIT predicts that the LCMS electron temperature variations are maintained within a narrow range around 40 eV, too small to be appreciated by the present measurement methods. In contrast, much larger variations are foreseen for the SOL ion temperature that is not measured in FTU, as in the large majority of tokamaks, because of the complex and largely perturbing apparatuses required [28]. Indeed, ions do not have power loss channels as effective as either conduction or radiation for electrons. The collisional coupling with electrons is also negligible in all the density regimes considered here and, consequently, the ion temperature is substantially higher than T_e. Figure 11 shows for the same discharges considered in figure 9, how much larger the predicted SOL T_i is, with respect to T_e, and how much greater is the effect on T_i of the different power flowing into the SOL.

No difference was found in the n_e, T_e values and D_α emission in the SOL between old and fresh boronization even at the highest additional power available in the experiment, namely 1.65 MW of LH. This is shown in figure 12, where the time evolution of total power, line averaged density, SOL electron density, D_α emission and Z_{eff} are compared for two discharges. The density rise, both in the main plasma and in the SOL, is very similar in both cases. The increase of n_e during the additional heating phase is due to the enhanced particle recycling from the wall, as evidenced by the rise of the D_α signal, and it is induced by the larger thermal load on the wall. The only significant difference found is in the Z_{eff}, value which is lower after a fresh boronization than after an old boronization, both in the ohmic and in the LH phases. The change induced by LH on $T_{e,SOL}$ has a small amplitude that is difficult to recognize from the temporal trace (not shown here), for the reasons given above.

4. Recycling properties and density control

During the first 60 discharges when the toroidal limiter is covered by the boron film, the wall can either pump or release a large amount of H and/or D, outside the operator control, depending on the degree of saturation of the surfaces facing the plasma as was previously observed after titanization [12]. This wall behaviour is evidenced in figure 13 by plotting N_p (the total plasma particle content) versus N_g (the total amount of the injected particles) for pre- and post-boronization discharges.

The ratio N_p/N_g is always well below 1.0, indicating that only a small fraction of the input gas is found in the discharge as plasma. Nevertheless, the amount of gas required to obtain similar density conditions may significantly change during the boronization phase (by a factor of 10). The lowest value of N_p/N_g (0.03) is obtained initially, since the boron film pumps strongly for the whole duration of the plasma discharge (1.5 s), and the pre-programmed density of $0.5 \times 10^{20}\,m^{-3}$ is not reached. The highest value (0.87) is obtained after several medium–high density discharges. In these conditions, the H or D particles released from the boron film strongly contribute to the plasma density. As a consequence, n_e increases well above the pre-programmed value of $0.4 \times 10^{20}\,m^{-3}$, i.e. up to $0.8 \times 10^{20}\,m^{-3}$, despite the gas being stopped by the feedback system at 0.3 s. When the walls are purely metallic, the variation of N_p/N_g is low (about a factor 3.2). The above effects are not observed after boronization if the plasma operations are performed at a low plasma density ($\bar{n}_e = 0.45 \times 10^{20}\,m^{-3}$), where almost reproducible wall conditions are obtained (see section 3.4).

In order to understand better the role of the chamber wall to the particle fuelling, a simple equilibrium equation can be derived: $dN_p/dt = dN_g/dt - dN_w/dt$, which relates the variation of the plasma content to the variation of the gas injected and the wall particles content. The last quantity can be expressed in terms of particle confinement time τ_p and the global recycling coefficient R, according to the relation: $dN_w/dt = N_p(1 - R)/\tau_p$ [29]. This formula is valid only for $0 \leqslant R \leqslant 1$, where the upper limit corresponds to wall saturation and allows the effective particle confinement time to be defined as $\tau_{eff} = \tau_p/(1 - R) = N_p/(dN_g/dt - dN_p/dt)$,

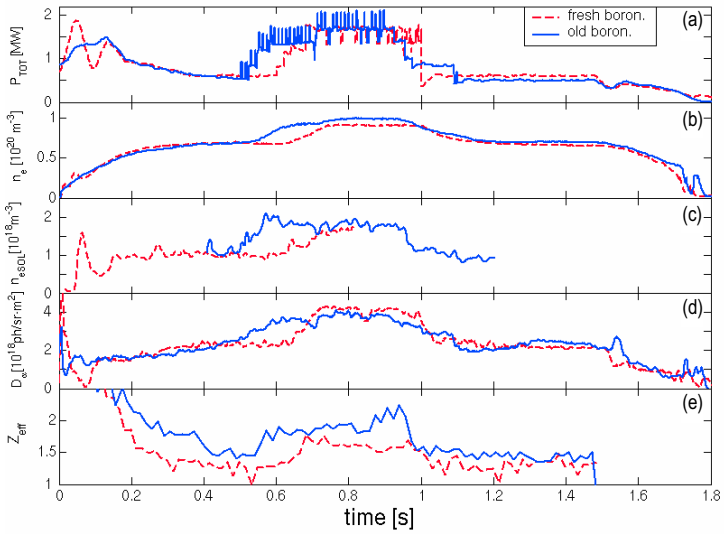

Figure 12. Temporal evolution of (*a*) total input power, (*b*) average electron density, (*c*) electron density in the SOL, (*d*) D_α emission and (*e*) $Z_{\rm eff}$ value after a fresh boronization (#21470; - - - -) and after an old boronization (#20739; ——). For both discharges $I_{\rm p} = 0.5$ MA and $P_{\rm LH} = 1.65$ MW.

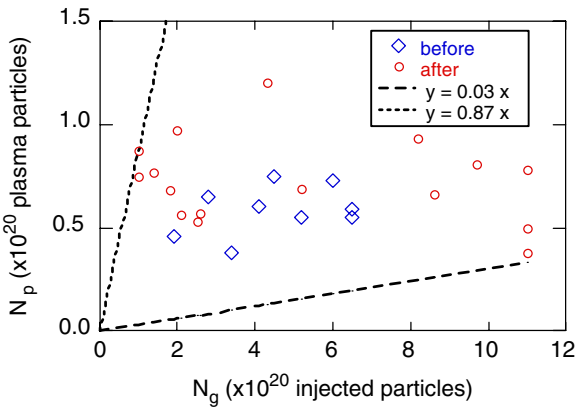

Figure 13. Plot of the total plasma particles $N_{\rm p}$ versus the total amount of injected particles $N_{\rm g}$. The dotted lines define the range of $N_{\rm p}/N_{\rm g}$ variation after boronization.

which takes into account, the influence of wall recycling on the plasma particle losses.

At fixed plasma current, the experimental $\tau_{\rm eff}$ ranges from 0.15 to 0.5 s before boronization, whereas it varies from 0.04 to 1.5 s after boronization. Figure 14 shows to what extent the boronization can influence the recycling, and hence the plasma–wall interaction for a high density pulse. The time evolution of plasma density, gas feed and D_α signal is indicated for a pulse performed one day after boronization. Even during the pulse, $\tau_{\rm eff}$ can strongly increase if the B layer reaches a saturation, as happens at $t = 1.0$ s in figure 14. During this shot the number of particles in the wall rises, as evidenced by the gas injection required to maintain the plasma density at a constant. The D_α signal increases up to about 1s and subsequently the total injected gas reaches a flat top, which indicates that no gas is fed by the valves. Therefore, the recycling coefficient at 1 s reaches a value very close to 1.

The above effects have not been observed on machines operating with high temperature walls, such as TEXTOR

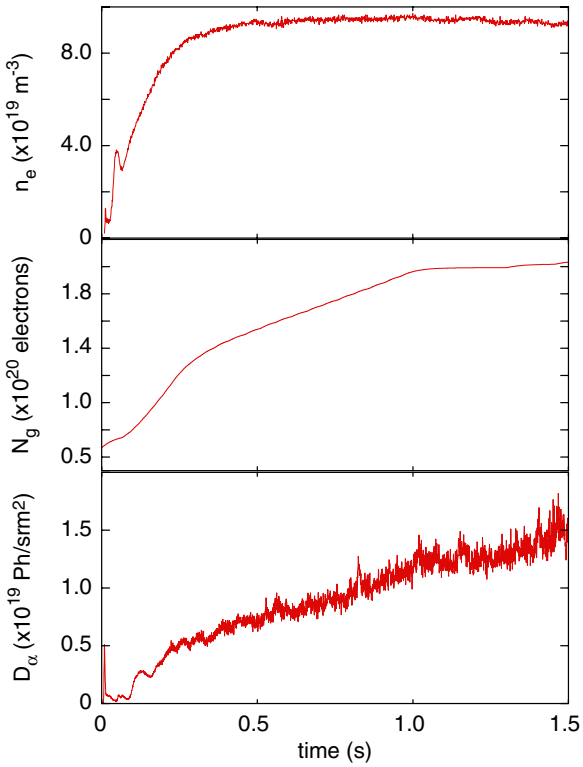

Figure 14. Time evolution of $\bar{n}_{\rm e}$, $N_{\rm g}$, D_α signal for a shot performed one day after boronization with $\bar{n}_{\rm e} = 0.9 \times 10^{20}$ m^{-3}, $I_{\rm p} = 0.5$ MA and $B_{\rm T} = 6$ T.

[30, 31], where the pumping and particle release mechanism of boron film has been clearly understood and optimized. FTU phenomenology can instead be explained by the strong modification of the plasma–wall interaction at very low surface temperature. Physical surface processes such as thermal diffusion and recombination of hydrogen atoms are not efficient at 77 K, and the most effective surface mechanisms are physical desorption induced by particle bombardment and high

pumping capability owing to the cold amorphous structure of the B layers. The latter, however, though quite high for the first few atomic monolayers, is counter-balanced by the extremely slow diffusion of the molecules absorbed into the bulk material. This, therefore, causes the surface to become quickly over-saturated under high particle flux until a strong desorption prevails after some pulses of this type. When this condition is reached, the subsequent plasma discharges are only fuelled by the gas released from the wall, and 2 or 3 shots are required before the wall partially recovers its pumping capability.

5. Conclusion

Boronization is very effective on FTU in reducing plasma contamination by oxygen on the whole plasma density regime $0.3 \leqslant \bar{n}_e \leqslant 3.2 \times 10^{20}\ m^{-3}$ and plasma currents $0.35 \leqslant I_p \leqslant 1.1$ MA and in extending plasma operation to very low electron density as required by some FTU experiments. Good results have also been obtained after 60 discharges after boronization, when the boron has been eroded from the limiter but is still present on the chamber wall. This is due to the reduction of metal influx because the physical sputtering by oxygen ions and atoms is strongly reduced and also because of the gettering effect of boron on oxygen, which maintains very clean plasmas for a long time (at least 500 plasma discharges).

Very low radiated power and Z_{eff} value have been obtained in both the ohmic and the LH and/or EC heated plasmas (up to 2.6 MW of total RF power injected) allowing the optimization of the plasma conditions for CD and internal transport barrier (ITB) experimental programmes [32]. The constraint in maintaining the FTU vessel temperature around 77 K leads to large differences in the recycling properties, immediately after boronization, with respect to purely metallic walls, which are the most suitable materials for plasma density control ($R < 1$). During this phase the best conditions for plasma reproducibility have been found only while operating at low density. At medium–high density instead, the wall can either pump or release a large amount of working gas depending on the saturation degree of the surfaces facing the plasma.

In conclusion, all the results indicate that boronization on a fully metallic and carbon-free machine at medium–high density regimes can be very useful for steady state operation owing to the long-lasting effect of boron on oxygen.

References

[1] Winter J. *et al* 1989 *J. Nucl. Mater.* **162–164** 713–23
[2] Rohde V. *et al* 1999 *26th EPS Conf. on Controlled Fusion and Plasma Physics (Maastricht, 14–18 June 1999)* vol 23J (ECA) pp 1513–16
[3] Saidoh M. *et al* 1993 *Japan. J. Appl. Phys.* **32** 3276–81
[4] Gauthier E. *et al* 1992 *J. Nucl. Mater.* **196–198** 637
[5] Phillips J. *et al* 1992 *J. Vac. Sci. Technol.* A **10** 1252
[6] Winter J. *et al* 1993 *Phys. Rev. Lett.* **71** 1549–52
[7] Marmar E.S. *et al* 1996 *Bull. Am. Phys. Soc.* **41** 1551
[8] De Marco F., Pieroni L., Santini S. and Segre S.E. 1986 *Nucl. Fusion* **26** 1193
[9] Kurz C. *et al* 1995 *J. Nucl. Mater.* **220–222** 963–6
[10] Apicella M.L. *et al* 1997 *Nucl. Fusion* **37** 381–96
[11] Apicella M.L. *et al* 1997 *Plasma Phys. Control. Fusion* **39** 1153–67
[12] Apicella M.L. *et al* 2000 *27th EPS Conf. on Controlled Fusion and Plasma Physics (Budapest, 12–16 June 2000)* vol 24B (ECA) pp 1573–6
[13] Apicella M.L. *et al* 2003 *J. Nucl. Mater.* **313–316** 269–73
[14] Angelini B. *et al* 2004 *FTU Operation* chapter 10, pp 437–58 (special issue on FTU) *Fusion Sci. Technol.* **45** 297–520
[15] Schneider U. *et al* 1990 *J. Nucl. Mater.* **176–177** 350–6
[16] Apicella M.L. *et al* 1994 *J. Nucl. Mater.* **212–215** 1541–5
[17] May M.J. *et al* 2001 *Phys. Rev.* E **64** 036406-1
[18] Pericoli-Ridolfini V. *et al* 1999 *Phys. Rev. Lett.* **82** 93
[19] Esposito B. *et al* 2004 *Transport Studies in the FTU Tokamak* chapter 6, pp 370–86 (special issue on FTU) *Fusion Sci. Technol.* **45** 297–520
[20] Kaye S.M. *et al* 1997 *Nucl. Fusion* **37** 1303
[21] Zagórski R., Romanelli F. and Pieroni L. 1996 *Nucl. Fusion* **36** 873
[22] Frigione D. *et al* 1996 *Nucl. Fusion* **36** 1489–99
[23] Post D.E. and Jensen R.V. 1977 *At. Data Nucl. Data Tables* **20** 397–439
[24] Pericoli Ridolfini V. *et al* 1995 *J. Nucl. Mater.* **220–222** 218
[25] Leigheb M., Pericoli Ridolfini V. and Zagórski R. 1997 *J. Nucl. Mater.* **241–243** 914
[26] Zagórski R., Pieroni L. and Pericoli Ridolfini V. 1996 *Contrib. Plasma Phys.* **36** 140
[27] Zagórski R. 1996 *J. Tech. Phys.* **37** 7
[28] Matthews G.F. 1984 *J. Phys. D: Appl. Phys.* **17** 2243–54
[29] Loarer T. *et al* 1994 *Proc. 21st EPS Eur. Conf. on Controlled Fusion and Plasma Physics (Montpellier, 1994)* vol 18B, p 754
[30] Winter J. 1989 *J. Nucl. Mater.* **161** 265–330
[31] Waelbroeck F. *et al* 1989 *J. Nucl. Mater.* **162–164** 496–502
[32] Gormezano C. *et al* 2004 *Highlights of the Physics Studies in the FTU* chapter 2, pp 303–322 (special issue on FTU) *Fusion Sci. Technol.* **45** 297–520